PROCEEDINGS OF SCIENCE

Low-energy limit of SMEFT applied to $\tau^- \to \pi^-\pi^0\nu_\tau$ decays

J.A. Miranda*
Departamento de Física, Centro de Investigación y de Estudios Avanzados del IPN,
Apdo. Postal 14-740,07000 Ciudad de México, México.
E-mail: jmiranda@fis.cinvestav.mx, proig@fis.cinvestav.mx

We perform an effective field theory analysis of the $\tau^- \to \pi^-\pi^0\nu_\tau$ decays, that includes the most general interactions between Standard Model fields up to dimension six, assuming left-handed neutrinos. This approach corresponds to the low-energy limit of the SMEFT, which is the EFT of the SM in absence of New Physics up to few TeV. We constrain as much as possible the necessary Standard Model hadronic input using chiral symmetry, dispersion relations, data and asymptotic QCD properties. As a result, we set precise (competitive with low-energy and LHC measurements) bounds on (non-standard) charged current tensor interactions, finding a very small preference for their presence, according to Belle data. Belle-II near future measurements can thus be very useful in either confirming or further restricting new physics tensor current contributions to these decays.

7th Annual Conference on Large Hadron Collider Physics - LHCP2019
20-25 May, 2019
Puebla, Mexico

*Speaker.

PoS(LHCP2019)029

1. Introduction

The Standard Model of particle physics [1–3] is one of the most successful theories that describes strong, weak and electromagnetic interactions. In order to test and search for departures from the SM we use effective field theories which provide us with a model-independent framework to parameterize possible New Physics at low energies.
The SMEFT [4, 5] is the effective field theory of the SM that realizes its symmetries, it is written as series of higher dimensional operators constructed with the SM fields,

$$\mathscr{L}_{SMEFT} = \mathscr{L}_{SM} + \sum \frac{\alpha_i}{\Lambda^2}\mathscr{O}_i^{(6)} + \sum \frac{\beta_i}{\Lambda^4}\mathscr{O}_i^{(8)}. \tag{1.1}$$

Since odd-dimensional operators violate both lepton number and baryon number, the contributions coming from these operators are expected to be very suppressed.
The SMEFT asumes a gap between the *vev* and the Λ scales ($v \ll \Lambda$), the last corresponds to the characteristic scale of NP, this seems to be a good hypothesis since there is no evidence of NP at the LHC.
There are 2499 dimension-six operators contributing to the SMEFT lagrangian, this quantity is enormously reduced when we neglect the effects of lepton-flavor violating (LFV) and flavor-changing neutral current (FCNC) operators.
Working at low energies, the heavy fields H, $W^\pm$ and Z bosons and heavy quarks ($q = c, b, t$) are integrated out of the theory. The effective couplings need to be run down since now the information of these heavy fields is also encoded in these couplings.
In this proceeding, we describe how the $\tau^- \to \pi^-\pi^0\nu_\tau$ decays can be used as a tool for the search of tensor interactions ($\hat{\varepsilon}_T$) at low energies. A full discussion and more details are found in Ref. [6].

2. Effective theory analysis of $\tau \to \nu_\tau \bar{u}d$

The $\mathscr{O}(1\,\text{GeV})$ effective lagrangian for semileptonic strangeness and lepton-flavor conserving charged current transitions which involves any lepton ($\ell = e, \mu, \tau$) and regards only left-handed neutrinos (the subscripts L(R) denote left-(right-)handed projection) is written as

$$\begin{aligned}\mathscr{L}_{CC} = -\frac{4G_F}{\sqrt{2}}\big[&(1+[v_L]_{\ell\ell})\bar{\ell}_L\gamma_\mu\nu_{\ell L}\bar{u}_L\gamma^\mu d_L + [v_R]_{\ell\ell}\bar{\ell}_L\gamma_\mu\nu_{\ell L}\bar{u}_R\gamma^\mu d_R \\ &+ [s_L]_{\ell\ell}\bar{\ell}_R\nu_{\ell L}\bar{u}_R d_L + [s_R]_{\ell\ell}\bar{\ell}_R\nu_{\ell L}\bar{u}_L d_R \\ &+ [t_L]_{\ell\ell}\bar{\ell}_R\sigma_{\mu\nu}\nu_{\ell L}\bar{u}_R\sigma^{\mu\nu}d_L\big] + h.c.,\end{aligned} \tag{2.1}$$

where G_F is the tree-level definition of the Fermi constant and $\sigma^{\mu\nu} \equiv i[\gamma^\mu, \gamma^\nu]/2$. $v_{L,R}$, $s_{L,R}$ and t_L are low-scale effective couplings, by setting $v_{L,R} = s_{L,R} = t_L = 0$ we recover the SM effective lagrangian. As usual, we select $\mu = 2\,\text{GeV}$ in the $\overline{\text{MS}}$ scheme.

By introducing equivalent couplings $\varepsilon_S = s_L + s_R$, $\varepsilon_P = s_L - s_R$, $\varepsilon_{L,R} = v_{L,R}$ and $\varepsilon_T = t_L$ we work in an advantageous framework with defined-parity states. Particularizing for the case of τ-lepton, we get the effective lagrangian for semileptonic transitions

$$\begin{aligned}\mathscr{L}_{CC} = -\frac{G_F}{\sqrt{2}}V_{ud}(1+\varepsilon_L+\varepsilon_R)\{&\bar{\tau}\gamma_\mu(1-\gamma^5)\nu_\tau\,\bar{u}\big[\gamma^\mu-(1-2\hat{\varepsilon}_R)\gamma^\mu\gamma^5\big]d\\ &+\bar{\tau}(1-\gamma^5)\nu_\tau\,\bar{u}(\hat{\varepsilon}_S-\hat{\varepsilon}_P\gamma^5)d\\ &+2\hat{\varepsilon}_T\,\bar{\tau}\sigma_{\mu\nu}(1-\gamma^5)\nu_\tau\,\bar{u}\sigma^{\mu\nu}d\}+h.c.,\end{aligned} \tag{2.2}$$

where $\hat{\varepsilon}_i \equiv \varepsilon_i/(1+\varepsilon_L+\varepsilon_R)$ for $i=R,S,P,T$. Working at linear order in the couplings, we are not sensitive to $\varepsilon_L+\varepsilon_R$ because it affects the overall normalization of the Fermi constant.

3. Semileptonic τ decay amplitude

For the $\tau^- \to \pi^-\pi^0\nu_\tau$ decays only vector, scalar and tensor currents contribute. The decay amplitude reads [1]

$$\begin{aligned}\mathscr{M} &= \mathscr{M}_V+\mathscr{M}_S+\mathscr{M}_T\\ &= \frac{G_F V_{ud}\sqrt{S_{EW}}}{\sqrt{2}}(1+\varepsilon_L+\varepsilon_R)\big[L_\mu H^\mu+\hat{\varepsilon}_S L H+2\hat{\varepsilon}_T L_{\mu\nu}H^{\mu\nu}\big],\end{aligned} \tag{3.1}$$

where the following lepton currents were introduced:

$$L_\mu = \bar{u}(P')\gamma^\mu(1-\gamma^5)u(P), \tag{3.2a}$$
$$L = \bar{u}(P')(1+\gamma^5)u(P), \tag{3.2b}$$
$$L_{\mu\nu} = \bar{u}(P')\sigma_{\mu\nu}(1+\gamma^5)u(P). \tag{3.2c}$$

The scalar (H), vector (H^μ) and tensor ($H^{\mu\nu}$) hadron matrix elements in eq. (3.1) can be constructed using Lorentz invariance and discrete QCD symmetries. Thus, these are

$$H = \langle\pi^0\pi^-|\bar{d}u|0\rangle \equiv F_S(s), \tag{3.3a}$$
$$H^\mu = \langle\pi^0\pi^-|\bar{d}\gamma^\mu u|0\rangle = C_V Q^\mu F_+(s)+C_S\left(\frac{\Delta_{\pi^-\pi^0}}{s}\right)q^\mu F_0(s), \tag{3.3b}$$
$$H^{\mu\nu} = \langle\pi^0\pi^-|\bar{d}\sigma^{\mu\nu}u|0\rangle = iF_T(s)(P^\mu_{\pi^0}P^\nu_{\pi^-}-P^\mu_{\pi^-}P^\nu_{\pi^0}). \tag{3.3c}$$

In this expressions F_S, F_+, F_0 and F_T are form factors, the hadronization procedure is encoded in these scalar functions. Taking the divergence of the vector current, eq. (3.3b), we can relate $F_S(s)$ with $F_0(s)$ via

$$F_S(s) = C_S\frac{\Delta_{\pi^-\pi^0}}{(m_d-m_u)}F_0(s). \tag{3.4}$$

As in Ref. [7], the scalar current can be absorbed in the vector current amplitude by making the following replacement

$$C_S\frac{\Delta_{\pi^-\pi^0}}{s} \longrightarrow C_S\frac{\Delta_{\pi^-\pi^0}}{s}\left[1+\frac{s\,\hat{\varepsilon}_S}{m_\tau(m_d-m_u)}\right], \tag{3.5}$$

[1] As in Ref. [7], we take the short-distance electroweak radiative corrections encoded in S_{EW} [8–15] as a global factor in eq. (3.1). Although S_{EW} does not affect the scalar and tensor contributions, the error of this approximation is negligible and renders simpler expressions than proceeding otherwise.

in eq. (3.3b).
Since form factors need to comply with analyticity and unitarity, we used previous results that employed a phase dispersive relation for the scalar [16], vector [17] and tensor [18,19] form factors implementing the known chiral constraints at low-energies and QCD asymptotics at short distances (high-energies).

4. Decay observables

To study the $\tau^- \to \pi^-\pi^0\nu_\tau$ decays we need to use as many observables as we can in order to search for possible NP effects. In this section we explore the effects of non-standard tensor and scalar interactions on the hadronic spectrum, branching ratio, Dalitz plot distributions and the measurable forward-backward asymmetry.
The differential decay width of the $\tau^- \to \pi^-\pi^0\nu_\tau$ decays, in the τ lepton rest frame, is

$$\frac{d^2\Gamma}{ds\,dt} = \frac{1}{32(2\pi)^3 M_\tau^3}\overline{|\mathscr{M}|^2}, \tag{4.1}$$

where $\overline{|\mathscr{M}|^2}$ represents the unpolarized spin-averaged squared matrix element, s is the $\pi^-\pi^0$ system invariant mass. The kinematic region is limited by $t^-(s) \le t \le t^+(s)$ and $(m_{\pi^0}+m_{\pi^-})^2 \le s \le M_\tau^2$, where

$$t^\pm(s) = \frac{1}{2s}\left[2s(M_\tau^2+m_{\pi^0}^2-s) - (M_\tau^2-s)(s+m_{\pi^-}^2-m_{\pi^0}) \pm (M_\tau^2-s)\sqrt{\lambda(s,m_{\pi^-}^2,m_{\pi^0}^2)}\right], \tag{4.2}$$

and $\lambda(x,y,z) = x^2+y^2+z^2-2xy-2xz-2yz$ is the Kallen function.
By using $t = m_{\pi^-}^2 + m_\tau^2 - 2E_\pi E_\tau + 2|\vec{p}_\pi||\vec{p}_\tau|\cos\theta$, where θ is the measurable angle between the momentum of the charged pion and the τ-lepton, we get the angular distribution (see Appx. B).

4.1 Dalitz Plots

The unpolarized spin-averaged squared amplitude that includes possible non-standard weak charged current interactions yields

$$\overline{|\mathscr{M}|^2} = \frac{G_F^2|V_{ud}|^2 S_{EW}}{s^2}(1+\varepsilon_L+\varepsilon_R)^2\left[M_{00}+M_{++}+M_{0+}+M_{T+}+M_{T0}+M_{TT}\right], \tag{4.3}$$

where M_{00}, M_{++} and M_{TT} correspond to scalar, vector, and tensor contributions respectively, and M_{0+}, M_{T+} and M_{T0} are their interferences. These expressions are in Appx. A. The scalar form factor is suppressed by a $\Delta_{\pi^-\pi^0}$ factor, which is small, leading to negligible effects even for $|\hat{\varepsilon}_S| \sim 1$. The Dalitz plot for the case of SM ($\hat{\varepsilon}_S = 0$, $\hat{\varepsilon}_T = 0$) is shown in fig. 1.

In order to appreciate the effects of non-vanishing $\hat{\varepsilon}_{S,T}$ in Dalitz plots, we introduce

$$\tilde{\Delta}(\hat{\varepsilon}_S,\hat{\varepsilon}_T) = \frac{\left|\overline{|\mathscr{M}(\hat{\varepsilon}_S,\hat{\varepsilon}_T)|^2} - \overline{|\mathscr{M}(0,0)|^2}\right|}{\overline{|\mathscr{M}(0,0)|^2}}. \tag{4.4}$$

Figures 2 and 3 show the $\tilde{\Delta}(\hat{\varepsilon}_S,\hat{\varepsilon}_T)$ plots for some representative values of $\hat{\varepsilon}_{S,T}$. In fig. 2, we take an unrealistic [2] value for $\hat{\varepsilon}_S$ setting $\hat{\varepsilon}_T = 0$ which is obtained from the $\tau^- \to \pi^-\pi^0\nu_\tau$ decays. In

[2] When it is compared to the bounds obtained from decays at low-energies and from colliders [7, 20, 21], if LU is assumed.

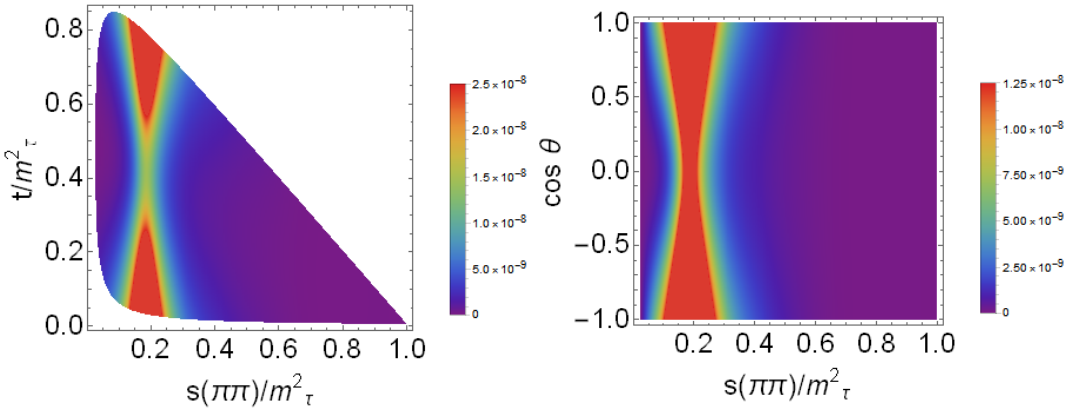

Figure 1: Dalitz plot distribution $\overline{|\mathscr{M}|^2}_{00}$ in the SM, eq. (4.3): Differential decay distribution for $\tau^- \to \pi^-\pi^0\nu_\tau$ in the (s,t) variables (left). The right-hand figure shows the differential decay distribution in the $(s, \cos\theta)$ variables, eq. (B.1). The Mandelstam variables, s and t, are normalized to M_τ^2.

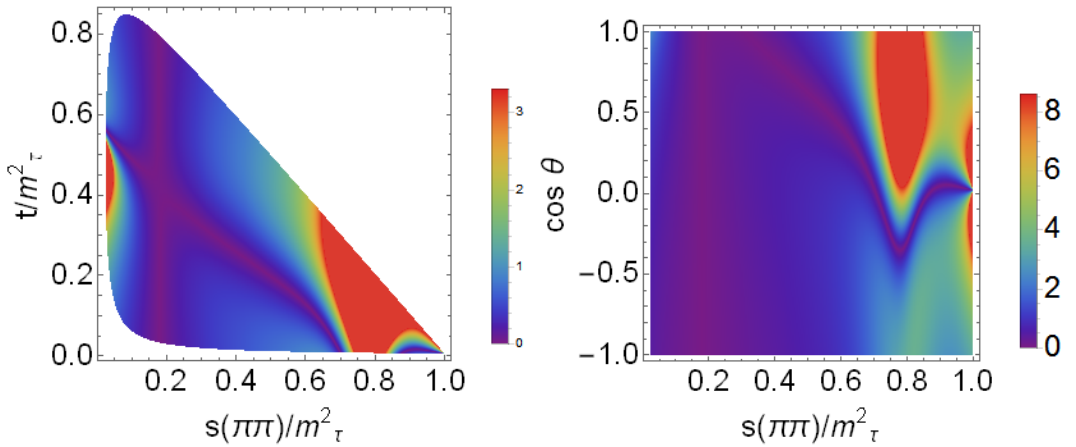

Figure 2: Dalitz plot distribution for $\tilde{\Delta}(\hat{\varepsilon}_S, \hat{\varepsilon}_T)$, (4.4), in the $\tau^- \to \pi^-\pi^0\nu_\tau$ decays: left-hand side corresponds to eq. (4.3) and right-hand side corresponds to the differential decay distribution in the $(s, \cos\theta)$ variables, both with $(\hat{\varepsilon}_S = 1.31, \hat{\varepsilon}_T = 0)$. The Mandelstam variables, s and t, are normalized to M_τ^2.

order to detect scalar interaction we need to measure Dalitz plots with an accuracy of $\sim 1\,\%$ (it is reduced to $\sim 0.1\,\%$ for a more realistic value). In fig. 3, we use a non-vanishing value for $\hat{\varepsilon}_T$ obtained from these decays setting $\hat{\varepsilon}_S = 0$, in order to appreciate the effects of tensor interactions we need to measure Dalitz plots with a precision of $\sim 0.1\,\%$. The same is true for the angular distribution.

4.2 Decay rate

By integrating upon the t variable in eq. (4.1), we get the $\pi^-\pi^0$ invariant mass distribution

$$\frac{d\Gamma}{ds} = \frac{G_F^2 |V_{ud}|^2 m_\tau^3 S_{EW}}{384\pi^3 s} (1+\varepsilon_L+\varepsilon_R)^2 \left(1-\frac{s}{m_\tau^2}\right)^2 \lambda^{1/2}\left(s, m_{\pi^0}^2, m_{\pi^-}^2\right) \times \left[X_{VA} + \hat{\varepsilon}_S X_S + \hat{\varepsilon}_T X_T + \hat{\varepsilon}_S^2 X_{S^2} + \hat{\varepsilon}_T^2 X_{T^2}\right]. \tag{4.5}$$

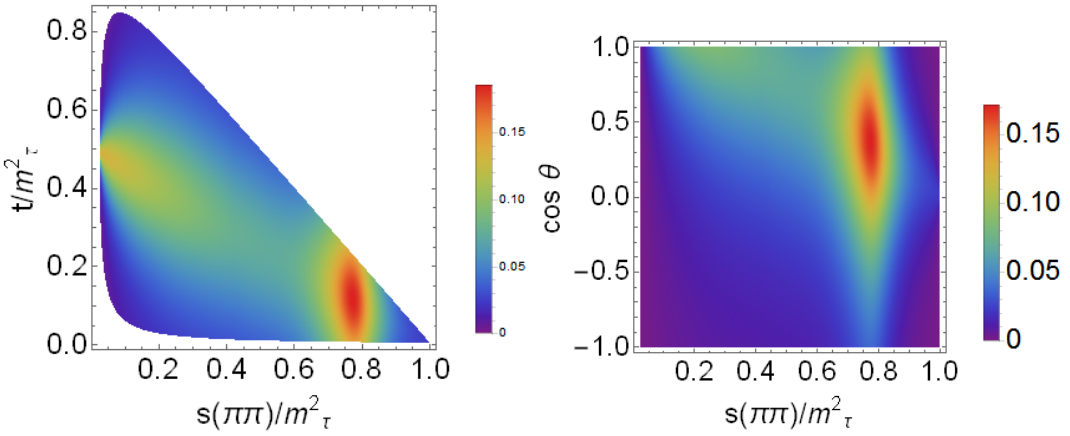

Figure 3: Dalitz plot distribution for $\tilde{\Delta}(\hat{\varepsilon}_S, \hat{\varepsilon}_T)$, (4.4), in the $\tau^- \to \pi^-\pi^0\nu_\tau$ decays: left-hand side corresponds to eq. (4.3) and right-hand side corresponds to the differential decay distribution in the $(s, \cos\theta)$ variables, both with $(\hat{\varepsilon}_S = 0, \hat{\varepsilon}_T = -0.014)$. The Mandelstam variables, s and t, are normalized to M_τ^2.

The expressions for X_{VA}, X_S, X_T, X_{S^2} and X_{T^2} are found in Appx. C. We recover the SM limit when $\varepsilon_L = \varepsilon_R = \hat{\varepsilon}_S = \hat{\varepsilon}_T = 0$. In fig. 4, this observable is plotted for a non-vanishing $\hat{\varepsilon}_S$ ($\hat{\varepsilon}_T$) . On the one hand, the deviation from the SM due to tensor interactions (dotted line) is very tiny. On the other hand, it seems that the deviation from the SM due to scalar interactions (dashed line) above 1.2 GeV is bigger but it corresponds to an unrealistic value for $\hat{\varepsilon}_S$, it goes away when we take into account a more realistic one, also we have to recall that this model is reliable up to 1 GeV.

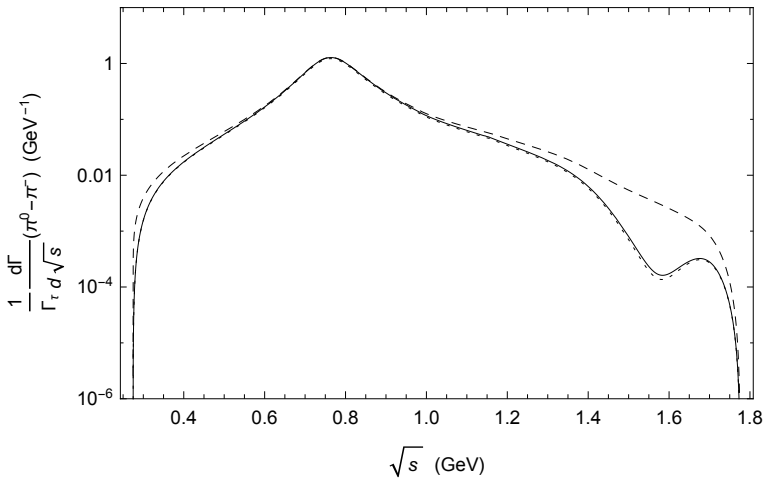

Figure 4: The $\pi^0\pi^-$ hadronic invariant mass distribution for the SM (solid line) and $\hat{\varepsilon}_S = 1.31, \hat{\varepsilon}_T = 0$ (dashed line), $\hat{\varepsilon}_S = 0, \hat{\varepsilon}_T = -0.014$ (dotted line). Axes units are given in GeV powers and the decay distributions are normalized to the tau decay width.

4.3 Forward-backward asymmetry

The forward-backward asymmetry for the $\tau^- \to \pi^-\pi^0\nu_\tau$ decays is given by

$$\mathscr{A}_{\pi\pi}(s) = \frac{-3C_S\sqrt{\lambda\left(s,m_{\pi^-}^2,m_{\pi^0}^2\right)}}{2s^2\left[X_{VA}+\hat{\varepsilon}_S X_S+\hat{\varepsilon}_T X_T+\hat{\varepsilon}_S^2 X_{S^2}+\hat{\varepsilon}_T^2 X_{T^2}\right]}\left(1+\frac{s\hat{\varepsilon}_S}{m_\tau(m_d-m_u)}\right)\Delta_{\pi^-\pi^0} \times\left\{C_V \mathrm{Re}[F_0(s)F_+^*(s)]+\frac{2s\,\hat{\varepsilon}_T}{m_\tau}\mathrm{Re}[F_T(s)F_0^*(s)]\right\}, \tag{4.6}$$

when we take $\hat{\varepsilon}_S = \hat{\varepsilon}_T = 0$ the SM forward-backward asymmetry is recovered, which agrees with the prediction in Ref. [16] (this asymmetry was firstly studied in Ref. [22]). This is plotted in fig. 5.

In fig. 6, we plot the forward-backward asymmetry for non-vanishing $\hat{\varepsilon}_{S,T}$. For tensor interactions

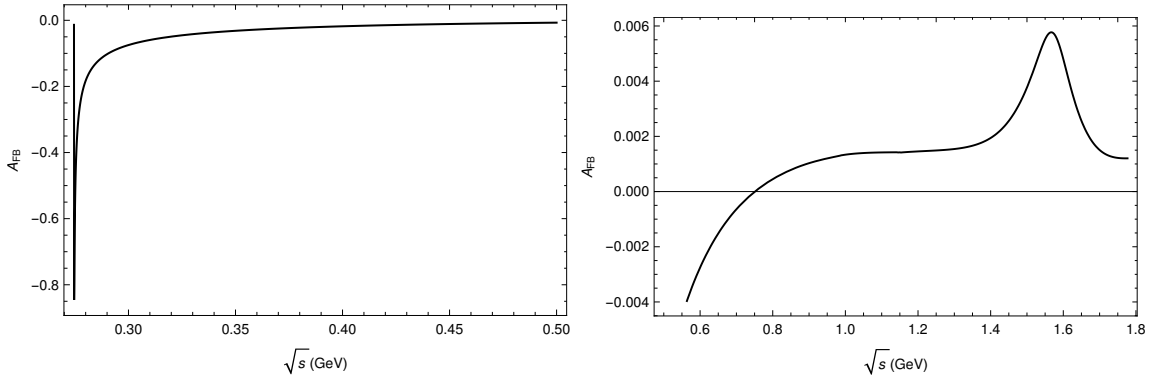

Figure 5: The forward-backward asymmetry in the $\tau^- \to \pi^-\pi^0\nu_\tau$ decay as a function of the $\pi\pi$ energy for the SM case. The low-energy region is shown in the left plot and remaining energy range is represented in the right plot.

(dotted line), we cannot distinguish their effects from the SM asymmetry distribution. In the case of scalar interactions, we have an enhancement with respect to the SM asymmetry but this distribution corresponds to an unrealistic value for $\hat{\varepsilon}_S$. This enhancement makes the forward-backward asymmetry an excellent observable to study non-standard scalar interactions. The deviation from

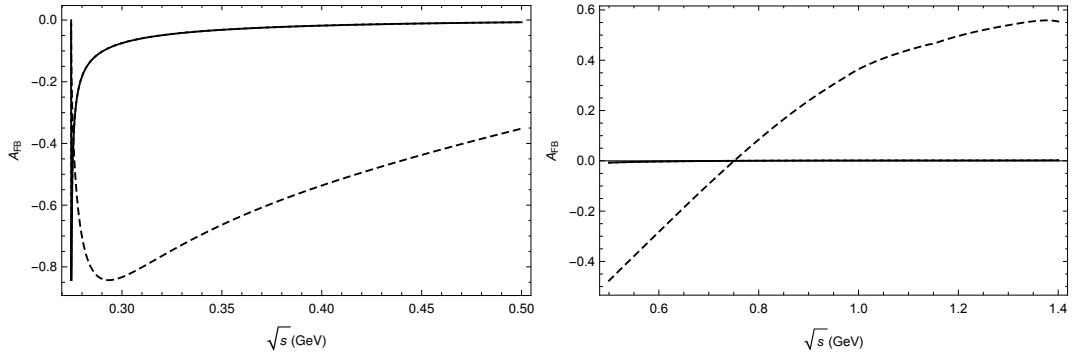

Figure 6: Forward-asymmetry for $\hat{\varepsilon}_S = 1.31, \hat{\varepsilon}_T = 0$ (dashed line) compared to the SM prediction (solid line). The left plot shows the low-energy region and the right plot includes the remaining energy range.

the SM asymmetry is plotted in fig. 7, where we have define ΔA_{FB} as

$$\Delta A_{FB} = A_{FB}(s,\hat{\varepsilon}_S,\hat{\varepsilon}_T) - A_{FB}(s,0,0). \tag{4.7}$$

In these plots, the effect due to scalar and tensor interactions is small even when we take into account more realistic values for $\hat{\varepsilon}_{S,T}$.

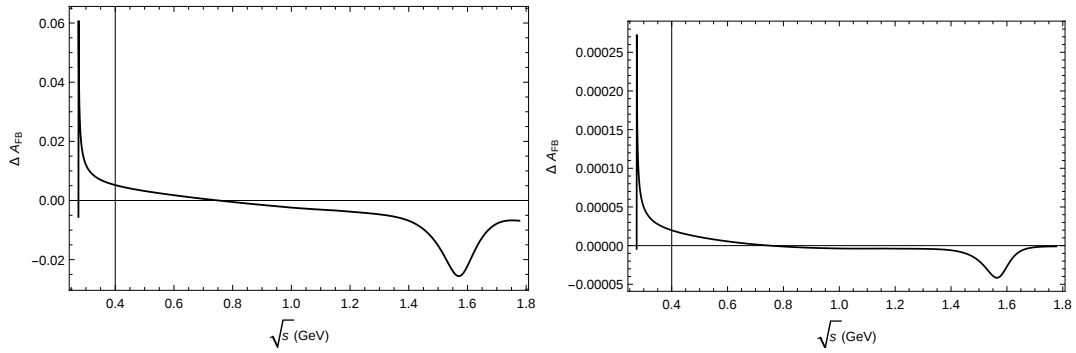

Figure 7: Normalized difference with respect to the SM for the forward-backward asymmetry (ΔA_{FB}) in the case of scalar interactions (left plot, with $\hat{\varepsilon}_S = 0.008, \hat{\varepsilon}_T = 0$) and tensor interactions (right plot, $\hat{\varepsilon}_T = -0.001, \hat{\varepsilon}_S = 0$).

5. Limits on $\hat{\varepsilon}_S$ and $\hat{\varepsilon}_T$

If we integrate the invariant mass distribution using the expressions for the form factors [16, 17], we get the $\tau^- \to \pi^-\pi^0\nu_\tau$ decay width as a function of the effective couplings. We can use it in order to set bounds on $\hat{\varepsilon}_S$ and $\hat{\varepsilon}_T$. For that, we measure the deviation due the effects of non-vanishing effective couplings (Γ) with respect to the SM limit (Γ^0) obtained neglecting them. Using the best fit results in ref. [17], we get a value for Γ^0 that corresponds to a branching fraction of $(25.53 \pm 0.24)\%$ which agrees with the PDG value of $(25.49 \pm 0.09)\%$. We measure the relative deviation produced by NP contributions as follows

$$\Delta \equiv \frac{\Gamma - \Gamma^0}{\Gamma^0} = \alpha\hat{\varepsilon}_S + \beta\hat{\varepsilon}_T + \gamma\hat{\varepsilon}_S^2 + \delta\hat{\varepsilon}_T^2\,, \tag{5.1}$$

where $\alpha = 3.5\times10^{-4}$, $\beta = 3.3^{+0.6}_{-0.4}$, $\gamma = 2.2\times10^{-2}$ and $\delta = 4.7^{+2.0}_{-1.0}$, these values take into account the theory error. Eq. (5.1) is a quadratic function of the effective couplings that can be used to set bounds on tensor and scalar interactions. First, we set a vanishing effective coupling $\hat{\varepsilon}_T$ ($\hat{\varepsilon}_S$) which let Δ as a function of the non-vanishing coupling $\hat{\varepsilon}_S$ ($\hat{\varepsilon}_T$). This is shown in fig. 8, the dotted line corresponds to the value of Δ using the current measurement for the branching ratio (at $3\,\sigma$ deviations) and the dashed line corresponds to an error reduced by a factor three, which could be achieve by Belle-II (the theory error is not assumed to decrease in this procedure). We get the following constraints: $-1.33 \le \hat{\varepsilon}_S \le 1.31$ with $\hat{\varepsilon}_T = 0$ and $[-0.79,-0.57]\cup[-1.4,1.3]\cdot10^{-2}$ for $\hat{\varepsilon}_T$ with $\hat{\varepsilon}_S = 0$. This values were used in the previous section.

We can also fix joint constraints on these effective couplings using the value of Δ obtained through the current measurement and the eq. (5.1), this is plotted in fig. 12 in Ref. [6]. These results are

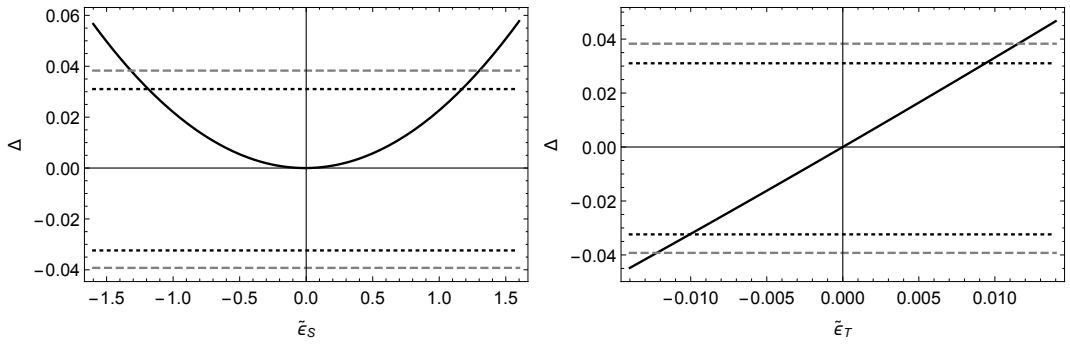

Figure 8: Δ as a function of $\hat{\varepsilon}_S$ for $\hat{\varepsilon}_T = 0$ (left-hand) and $\hat{\varepsilon}_T$ for $\hat{\varepsilon}_S = 0$ (right-hand) for $\tau^- \to \pi^-\pi^0\nu_\tau$ decays. Horizontal lines represent the values of Δ according to the current measurement and theory error (at three standard deviations) of the branching ratio (dashed line) and the hypothetical case of this value being measured by Belle-II with three times reduced error (dotted line).

Δ limits	$\hat{\varepsilon}_S\,(\hat{\varepsilon}_T = 0)$	$\hat{\varepsilon}_T\,(\hat{\varepsilon}_S = 0)$	$\hat{\varepsilon}_S$	$\hat{\varepsilon}_T$
Belle	$[-1.33, 1.31]$	$[-0.79, -0.57] \cup [-1.4, 1.3] \cdot 10^{-2}$	$[-5.2, 5.2]$	$[-0.79, 0.013]$
3-fold improved measurement	$[-1.20, 1.18]$	$[-0.79, -0.57] \cup [-1.1, 1.1] \cdot 10^{-2}$	$[-5.1, 5.1]$	$[-0.78, 0.011]$

Table 1: Constraints on the scalar and tensor couplings obtained (at three standard deviations) through the limits on the current branching ratio measurements and the hypothetical case where this value be measured by Belle II with a three times smaller error. Theory errors are included.

summarized in table 1.

Using the normalized spectrum $(1/N_{\pi\pi})(dN_{\pi\pi}/ds)$ reported by Belle [23] and the current branching ratio, we performed a fit using the funtion

$$\frac{1}{\Gamma(\hat{\varepsilon}_S, \hat{\varepsilon}_T)} \frac{d\Gamma(s, \hat{\varepsilon}_S, \hat{\varepsilon}_T)}{ds}. \tag{5.2}$$

We get $\hat{\varepsilon}_T = (-1.3^{+1.5}_{-2.2}) \cdot 10^{-2}$ restricting $|\hat{\varepsilon}_S| < 0.8 \times 10^{-2}$ [20, 21], which shows a slight preference (0.9 σ) to charged current tensor interactions.

Finally, if we assume LU it is possible to compared the results obtained from the $\tau^- \to \pi^-\pi^0\nu_\tau$ decays with those obtained from low-energy processes and colliders [7, 20, 21]. For scalar interactions, we found $|\hat{\varepsilon}_S| < 1.3$ while the limit from low-energy decays is $|\hat{\varepsilon}_S| < 0.34 \times 10^{-2}$ (at 90 % C.L.). On the other hand, we get $\hat{\varepsilon}_T = (-1.3^{+1.5}_{-2.2}) \cdot 10^{-2}$ for tensor interactions which is a very competitive constraint when it is compared to $|\hat{\varepsilon}_T| < 0.1 \times 10^{-2}$ (at 90 % C.L.) obtained from radiative pion decays reported in Refs. [20, 21].

Through an analysis of inclusive and exclusive τ decays [24], it is possible to set constraints on the other effective couplings in eq. (2.2). They get $\hat{\varepsilon}_S^\tau = (-0.6 \pm 1.5) \cdot 10^{-2}$ and $\hat{\varepsilon}_T^\tau = (-0.04 \pm 0.46) \cdot 10^{-2}$ for the scalar and tensor couplings which are compatible with our results in this work and in Ref. [7].

6. Conclusions

Since the $\tau^- \to \pi^-\pi^0\nu_\tau$ decays have the largest branching ratio, we can study these decays in a model independent effective theory framework. Within this framework, we have set bounds on $\hat{\varepsilon}_S$ and $\hat{\varepsilon}_T$ using the measured Belle branching ratio, through the observable Δ. This yields quite competitive constraints with the world-best bounds for the tensor case, but quite poor in the scalar case due to the isospin suppression factor ($\Delta_{\pi^-\pi^0}$).
Accordingly to these results, the Dalitz plot distributions and the forward-backward asymmetry are not very sensitive to non-vanishing realistic values of $\hat{\varepsilon}_S$ and $\hat{\varepsilon}_T$. The hadronic invariant mass distribution is not sensitive to charged-current tensor interactions but a fit to the Belle spectrum shows a slight preference for non-zero $\hat{\varepsilon}_T$. Hence, it is very worth to measure with extreme precision the $\pi\pi$ invariant mass distribution in $\tau^- \to \pi^-\pi^0\nu_\tau$ decays at Belle-II in order to further restrict $\hat{\varepsilon}_T$ and provide complementary information to other low-energy decays searching for non-standard interactions.

References

[1] S. L. Glashow, *The renormalizability of vector meson interactions*, *Nucl. Phys.* **10** (1959) 107.

[2] A. Salam and J. C. Ward, *Weak and electromagnetic interactions*, *Nuovo Cim.* **11** (1959) 568.

[3] S. Weinberg, *A Model of Leptons*, *Phys. Rev. Lett.* **19** (1967) 1264.

[4] W. Buchmuller and D. Wyler, *Effective Lagrangian Analysis of New Interactions and Flavor Conservation*, *Nucl. Phys.* **B268** (1986) 621.

[5] B. Grzadkowski, M. Iskrzynski, M. Misiak and J. Rosiek, *Dimension-Six Terms in the Standard Model Lagrangian*, *JHEP* **10** (2010) 085 [1008.4884].

[6] J. A. Miranda and P. Roig, *Effective-field theory analysis of the $\tau^- \to \pi^-\pi^0\nu_\tau$ decays*, *JHEP* **11** (2018) 038 [1806.09547].

[7] E. A. Garcés, M. Hernández Villanueva, G. López Castro and P. Roig, *Effective-field theory analysis of the $\tau^- \to \eta^{(\prime)}\pi^-\nu_\tau$ decays*, *JHEP* **12** (2017) 027 [1708.07802].

[8] A. Sirlin, *Radiative corrections to g(v)/g(mu) in simple extensions of the su(2) x u(1) gauge model*, *Nucl. Phys.* **B71** (1974) 29.

[9] A. Sirlin, *Current Algebra Formulation of Radiative Corrections in Gauge Theories and the Universality of the Weak Interactions*, *Rev. Mod. Phys.* **50** (1978) 573.

[10] A. Sirlin, *Large m(W), m(Z) Behavior of the O(alpha) Corrections to Semileptonic Processes Mediated by W*, *Nucl. Phys.* **B196** (1982) 83.

[11] W. J. Marciano and A. Sirlin, *Radiative Corrections to beta Decay and the Possibility of a Fourth Generation*, *Phys. Rev. Lett.* **56** (1986) 22.

[12] W. J. Marciano and A. Sirlin, *Electroweak Radiative Corrections to tau Decay*, *Phys. Rev. Lett.* **61** (1988) 1815.

[13] W. J. Marciano and A. Sirlin, *Radiative corrections to pi(lepton 2) decays*, *Phys. Rev. Lett.* **71** (1993) 3629.

[14] E. Braaten and C.-S. Li, *Electroweak radiative corrections to the semihadronic decay rate of the tau lepton*, *Phys. Rev.* **D42** (1990) 3888.

[15] J. Erler, *Electroweak radiative corrections to semileptonic tau decays*, *Rev. Mex. Fis.* **50** (2004) 200 [hep-ph/0211345].

[16] S. Descotes-Genon and B. Moussallam, *Analyticity of $\eta\pi$ isospin-violating form factors and the $\tau \to \eta\pi\nu$ second-class decay*, *Eur. Phys. J.* **C74** (2014) 2946 [1404.0251].

[17] D. Gómez Dumm and P. Roig, *Dispersive representation of the pion vector form factor in $\tau \to \pi\pi\nu_\tau$ decays*, *Eur. Phys. J.* **C73** (2013) 2528 [1301.6973].

[18] V. Cirigliano, A. Crivellin and M. Hoferichter, *No-go theorem for nonstandard explanations of the $\tau \to K_S\pi\nu_\tau$ CP asymmetry*, *Phys. Rev. Lett.* **120** (2018) 141803 [1712.06595].

[19] J. Rendón, P. Roig and G. Toledo Sánchez, *Effective-field theory analysis of the $\tau^- \to (K\pi)^-\nu_\tau$ decays*, *Phys. Rev.* **D99** (2019) 093005 [1902.08143].

[20] V. Cirigliano, J. Jenkins and M. Gonzalez-Alonso, *Semileptonic decays of light quarks beyond the Standard Model*, *Nucl. Phys.* **B830** (2010) 95 [0908.1754].

[21] T. Bhattacharya, V. Cirigliano, S. D. Cohen, A. Filipuzzi, M. Gonzalez-Alonso, M. L. Graesser et al., *Probing Novel Scalar and Tensor Interactions from (Ultra)Cold Neutrons to the LHC*, *Phys. Rev.* **D85** (2012) 054512 [1110.6448].

[22] D.-N. Gao, *Angular distribution asymmetry in tau- —> pi- pi0 nu(tau) decay in the two-Higgs-doublet model with large tan beta*, *Phys. Rev.* **D71** (2005) 051301 [hep-ph/0411284].

[23] BELLE collaboration, *High-Statistics Study of the tau- —> pi- pi0 nu(tau) Decay*, *Phys. Rev.* **D78** (2008) 072006 [0805.3773].

[24] V. Cirigliano, A. Falkowski, M. González-Alonso and A. Rodríguez-Sánchez, *Hadronic τ Decays as New Physics Probes in the LHC Era*, *Phys. Rev. Lett.* **122** (2019) 221801 [1809.01161].

A. Unpolarized spin-averaged squared amplitude

The scalar, vector, tensor and interference amplitude read

$$
\begin{aligned}
M_{0+} &= 2C_V\,C_S\,m_\tau^2\,\mathrm{Re}\left[F_+(s)F_0^*(s)\right]\,\Delta_{\pi^-\pi^0}\left(1+\frac{s\hat{\varepsilon}_S}{m_\tau(m_d-m_u)}\right)\\
&\quad\times\left\{s\left(m_\tau^2-s-2t+\Sigma_{\pi^-\pi^0}\right)-m_\tau^2\Delta_{\pi^-\pi^0}\right\},\\
M_{T+} &= 4C_V\,\hat{\varepsilon}_T\,m_\tau^3\,s\,\mathrm{Re}\left[F_T(s)F_+^*(s)\right]\left(1-\frac{s}{m_\tau^2}\right)\lambda(s,m_{\pi^-}^2,m_{\pi^0}^2),\\
M_{T0} &= 4C_S\,\Delta_{\pi^-\pi^0}\,\hat{\varepsilon}_T\,m_\tau\,s\,\mathrm{Re}\left[F_T(s)F_0^*(s)\right]\left(1+\frac{s\hat{\varepsilon}_S}{m_\tau(m_d-m_u)}\right)\\
&\quad\times\left\{s\left(m_\tau^2-s-2t+\Sigma_{\pi^-\pi^0}\right)-m_\tau^2\Delta_{\pi^-\pi^0}\right\},\\
M_{00} &= C_S^2\,\left(\Delta_{\pi^-\pi^0}\right)^2 m_\tau^4\left(1-\frac{s}{m_\tau^2}\right)|F_0(s)|^2\left(1+\frac{s\hat{\varepsilon}_S}{m_\tau(m_d-m_u)}\right)^2,\\
M_{++} &= C_V^2\,|F_+(s)|^2\Bigg\{m_\tau^4\left(s-\Delta_{\pi^-\pi^0}\right)^2-m_\tau^2 s\left[s(s+4t)-2\Delta_{\pi^-\pi^0}\left(s+2t-\Sigma_{\pi^-\pi^0}\right)+\left(\Delta_{\pi^-\pi^0}\right)^2\right]\\
&\qquad+4m_{\pi^-}^2 s^2\left(m_{\pi^0}^2-t\right)+4s^2t\left(s+t-m_{\pi^0}^2\right)\Bigg\},\\
M_{TT} &= 4\hat{\varepsilon}_T^2\,|F_T(s)|^2 s^2\Bigg\{m_{\pi^-}^4\left(m_\tau^2-s\right)-2m_{\pi^-}^2\left(m_\tau^2-s\right)\left(s+2t-m_{\pi^0}^2\right)-m_{\pi^0}^4\left(3m_\tau^2+s\right)\\
&\qquad+2m_{\pi^0}^2\left[\left(s+m_\tau^2\right)(s+2t)-2m_\tau^4\right]-s\left[(s+2t)^2-m_\tau^2(s+4t)\right]\Bigg\},
\end{aligned}
\tag{A.1}
$$

where the familiar definitions $\Delta_{\pi^-\pi^0}=m_{\pi^-}^2-m_{\pi^0}^2$ and $\Sigma_{\pi^-\pi^0}=m_{\pi^-}^2+m_{\pi^0}^2$ were employed.

B. Angular distribution

The decay distribution in the $(s,\cos\theta)$ variables, for $\hat{\varepsilon}_S$ and $\hat{\varepsilon}_T$ is

$$
\begin{aligned}
\frac{d^2\Gamma}{d\sqrt{s}\,d\cos\theta} &= \frac{G_F^2|V_{ud}|^2 S_{EW}}{128\pi^3 m_\tau}(1+\varepsilon_L+\varepsilon_R)^2\left(\frac{m_\tau^2}{s}-1\right)^2|\vec{p}_{\pi^-}|\Bigg\{C_S^2\left(\Delta_{\pi^-\pi^0}\right)^2|F_0(s)|^2\\
&\quad\times\left(1+\frac{s\hat{\varepsilon}_S}{m_\tau(m_d-m_u)}\right)^2+16|\vec{p}_{\pi^-}|^2 s^2\left|\frac{C_V}{2m_\tau}F_+(s)+\hat{\varepsilon}_T F_T(s)\right|^2\\
&\quad+4|\vec{p}_{\pi^-}|^2 s\left(1-\frac{s}{m_\tau^2}\right)\cos^2\theta\left[C_V^2|F_+(s)|^2-4s\hat{\varepsilon}_T^2|F_T(s)|^2\right]-4C_S\Delta_{\pi^-\pi^0}|\vec{p}_{\pi^-}|\sqrt{s}\cos\theta\\
&\quad\times\left(1+\frac{s\hat{\varepsilon}_S}{m_\tau(m_d-m_u)}\right)\left[C_V\mathrm{Re}\left[F_0(s)F_+^*(s)\right]+\frac{2s\hat{\varepsilon}_T}{m_\tau}\mathrm{Re}\left[F_T(s)F_0^*(s)\right]\right]\Bigg\},
\end{aligned}
\tag{B.1}
$$

which coincides with the SM result when $\hat{\varepsilon}_{S,T}$ are set to zero.

C. Decay rate

$$X_{VA} = \frac{1}{2s^2}\left[3|F_0(s)|^2 C_S^2 \Delta^2_{\pi^-\pi^0} + |F_+(s)|^2 C_V^2 \left(1+\frac{2s}{m_\tau^2}\right)\lambda\left(s, m^2_{\pi^0}, m^2_{\pi^-}\right)\right], \tag{C.1a}$$

$$X_S = \frac{3}{s\, m_\tau}|F_0(s)|^2 C_S^2 \frac{\Delta^2_{\pi^-\pi^0}}{m_d - m_u}, \tag{C.1b}$$

$$X_T = \frac{6}{s\, m_\tau}\mathrm{Re}\left[F_T(s) F_+^*(s)\right] C_V \lambda\left(s, m^2_{\pi^0}, m^2_{\pi^-}\right), \tag{C.1c}$$

$$X_{S^2} = \frac{3}{2m_\tau^2}|F_0(s)|^2 C_S^2 \frac{\Delta^2_{\pi^-\pi^0}}{(m_d - m_u)^2}, \tag{C.1d}$$

$$X_{T^2} = \frac{4}{s}|F_T(s)|^2 \left(1+\frac{s}{2m_\tau^2}\right)\lambda\left(s, m^2_{\pi^0}, m^2_{\pi^-}\right). \tag{C.1e}$$